Dipolar rotor-rotor interactions in a difluorobenzene molecular rotor crystal

Robert D. Horansky, Laura I. Clarke,* Erick B. Winston, and John C. Price
Department of Physics, University of Colorado, Boulder, Colorado 80309, USA

Steven D. Karlen, Peter D. Jarowski, Rosa Santillan,† and Miguel A. Garcia-Garibay
Department of Chemistry and Biochemistry, University of California, Los Angeles, California 90095, USA
(Received 19 January 2006; revised manuscript received 23 June 2006; published 31 August 2006)

In this paper, we characterize the rotational dynamics and observe rotor-rotor interactions within a crystalline, three-dimensional array of dipolar molecular rotors. The rotating portion of each rotor molecule consists of a dipolar fluorine-substituted phenyl group. The phenyl rotors are connected by acetylene linkages to bulky triphenyl methyl groups which are held rigid in the crystal lattice. These custom synthesized rotor molecules allow control over the molecular spacing in the lattice, the dipole strength, and the rotational hindrance, thus permitting formation of systems with rapid thermal rotation and strong dipole-dipole interactions, which is of interest for studying new phases and collective phenomena. Dielectric and ^{2}H NMR spectroscopy measurements are used to map the rotational potential, and to explore the influence of rotor-rotor interactions. Interactions due to dipole-dipole effects are studied using a Monte Carlo simulation, while contributions from steric interactions between rotors are investigated using molecular mechanics methods. Both contributions are needed explain the dielectric spectroscopy results.

DOI: 10.1103/PhysRevB.74.054306 PACS number(s): 77.22.Gm, 77.84.−s, 81.07.−b, 81.07.Nb

I. INTRODUCTION

Molecular scale machinery provides an avenue for the study of physics at the nanometer range and for miniaturizing applications.[1–4] An example is the molecular rotor.[3–9] Dipolar molecular rotors are custom designed and synthesized molecules, sometimes referred to as molecular compasses,[8,9] with a subgroup containing a permanent electric dipole moment that rotates relative to another part of the molecule, which is rendered stationary by either attachment to a surface[7] or incorporation within a crystal.[6,8,9] By studying ordered arrays of these rotating dipoles, interesting physical phenomena may be observed. For example, it is predicted that 2D square and triangular arrays of rotating dipoles will exhibit Goldstone modes in which the ground state does not depend on the direction of polarization.[10] Other 2D arrangements are expected to yield interesting orientational phase transitions.[11] In addition, arrays of rotors could propagate molecular rotary waves at speeds much lower than typical phonon velocities.[12] This behavior might have application to radio frequency filters similar to those that now employ surface acoustic waves. Techniques of crystal design[13–18] may allow precise control over geometry and hence rotor-rotor dipolar interactions.

Molecular rotation has previously been studied in three-dimensional crystalline solids, which fall roughly into three categories. The first is inclusion compounds where the rotational barriers are typically very large compared to covalently bonded rotors.[19–21] The second type of solid rotor compounds are plastic crystals which differ from dipolar molecular rotors in that no rigid axle constrains the motion of the molecules, and the temperature where rotation takes place is near the melting point of the compound.[22–26] Finally, rotation of ionic groups within a crystal structure giving rise to dipolar ordering has also been studied.[21,27,28] In these systems, interactions between the rotating molecule and its local surroundings fully determine molecular dynamics, creating innate correlations between the bulk properties of the solid or crystal and the rotational motion. In principle, the synthetically designed molecular system presented here allows tuning of the rotational dynamics independent of bulk crystal properties due to the presence of a well-defined axle about which the rotator turns.

We previously studied a noninteracting system of dipolar crystalline rotors where the rotors were hindered by steric interactions with the surrounding crystal lattice.[6] This paper explores an analogous structure in which the rotating group has a larger dipole moment and rotor-rotor interactions are enhanced. The previous study used crystals made from molecules of 1,4-bis(3,3,3-triphenylpropynyl)-2-fluorobenzene (referred to as ROT-F) which is shown in Fig. 1. The ROT-F molecules were designed with a shape such that sufficient free space exists for the central phenylene, shown in black in Fig. 1, to experience rapid rotary motion along the axis of the triple bonds while the three phenyl groups remain stationary in the rigid crystal lattice. Since it is known that rotation about phenyl-alkyne bonds is essentially barrierless in the

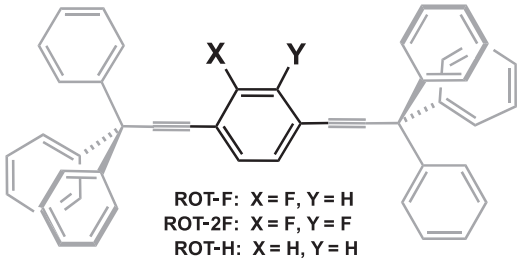

FIG. 1. The chemical structure of the synthesized rotor molecule is shown in three forms: the single fluorine containing ROT-F, the two fluorine containing ROT-2F, and the nonpolar ROT-H used as a control molecule. The rotary portion of the molecule is shown in black, while the stationary triphenyl groups that form the crystal superlattice are shown in gray.

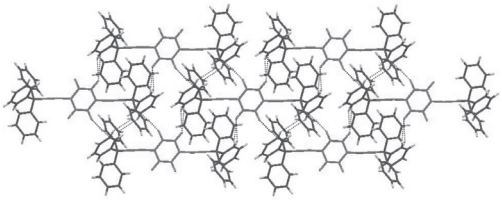

FIG. 2. The x-ray structure of ROT-2F is isomorphous with those of ROT-H and ROT-F. The crystal lattice is triclinic with a =9.18 Å, b=10.54 Å, c=10.55 Å, and α=62.74°, β=70.90°, γ =85.37°.

gas phase,[29,30] it was expected that any barrier seen in the crystal should be due to steric interactions from contacts with neighboring molecules, or to dipole-dipole effects. We showed that crystals of ROT-F are isomorphous with those of the nonpolar analog 1,4-bis(3,3,3-triphenylpropynyl)-benzene (referred to as ROT-H and shown in Fig. 1), and that the central rotating group of each molecule is subject to a rotational potential with two minima separated by 180°.[6,8,9] Molecules of ROT-H pack in the triclinic space group $P\bar{1}$ with only one molecule per unit cell as a result of coincident crystallographic and molecular inversion centers (Fig. 2). The 180° rotation of the central phenyl group is equivalent to an inversion of the molecule leading to a symmetric rotational potential, independent of the orientation of neighboring molecules in the crystal. However, for ROT-F, which also packs in the $P\bar{1}$ space group, the molecular inversion center is removed by the presence of a fluorine atom, as seen by the positional disorder of the fluorine location in the crystal structure about the former inversion center.[9]

An important consequence of the removal of inversion symmetry at the molecular level in ROT-F is that structures related by 180° rotation are no longer equivalent to an inversion, although the steric environment of the molecular rotor is still inversion symmetric when the positions of the surrounding rotors are rotationally averaged. This results in nonequivalent energy minima in the rotational potential. A schematic of the potential energy curve and its relation to the packing environment are shown in Fig. 3 in terms of an asymmetry parameter S and an energy barrier E_B in the solid potential curve. The steric interactions between the fluorophenylene rotator and surrounding molecules in the crystal are represented above each well by an inversion symmetric dashed line. Dielectric spectroscopy, ^{2}H NMR, and force field calculations in ROT-F indicated a barrier of $E_B \approx 12-14$ kcal/mol and an asymmetry parameter $S \approx 0.9-1.5$ kcal/mol depending on the crystallinity of the sample measured. In addition, there may be contributions to the energy asymmetry due to the actual orientations of the neighboring molecular dipoles, however, analysis of the calculational data showed these effects to be minimal and that these polar rotors are only subject to local steric effects. Therefore, the ROT-F rotors were in a dilute limit, with long enough distances for dipolar rotor-rotor interactions to play no role.

In this paper we report evidence of direct rotor-rotor interactions in crystals of 1,4-bis(3,3,3-triphenylpropynyl)-2,3-difluorobenzene (referred to as ROT-2F), which is shown in Fig. 1. ROT-2F is an analogous molecular rotor with an isomorphous crystal structure and a similar rotational barrier to ROT-F and ROT-H, but contains a larger dipole moment of $\mu \approx 3.0$ Debye perpendicular to the axis of rotation as compared to $\mu \approx 1.5$ Debye in ROT-F. Being isomorphous with ROT-H, the molecular and crystallographic inversion centers required by the space group of ROT-2F are coincident only on average, so that ROT-2F packs orientationally disordered with no preference for either of two symmetrically related wells. The equivalent orientations upon 180° rotation are shown for ROT-2F in Fig. 3, where the interaction with the surrounding crystal is represented by dashed lines. The observed x-ray structure can not exclude the possibility of local ordering.

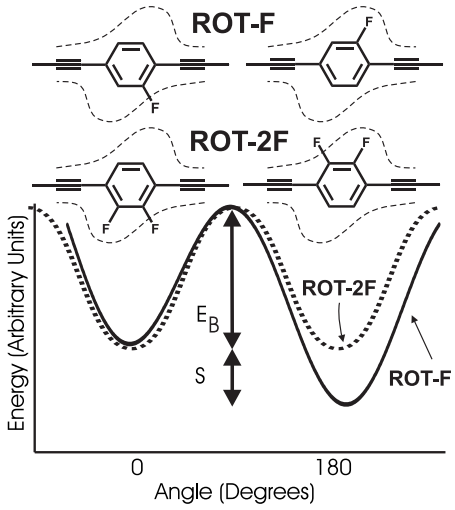

FIG. 3. Comparison of potential curves between the sterically asymmetric ROT-F, solid potential curve, and the sterically symmetric ROT-2F rotor, dashed potential curve. The dashed lines around the rotors represent the steric interactions of the surrounding crystal lattice and are inversion symmetric about the center of the rotating phenyl ring. The potential minima are located at 0° and 180°. The difference in well energies at these two angles is the asymmetry S and the lowest barrier to rotation is defined as E_B.

The asymmetry S in the ROT-F case was measurable because it has the effect of causing a substantial reduction in the dielectric loss signal magnitude as the measurement temperature is lowered and the equilibrium population of rotationally responsive molecules decreases. The asymmetry of the rotational potential in this case was attributed to local steric hindrance alone. However, if the steric asymmetry is removed, as is the case with ROT-2F, an effective asymmetry causing a similar reduction in the dielectric loss signal magnitude could be ascribed to orientationally dependent dipole-dipole interactions, as will be shown in Sec. IV E. Thus, the presence of a rotating, relatively large permanent dipole moment in ROT-2F is ideal for investigation of the rotational behavior by dielectric spectroscopy. The possibility of dipole-dipole interactions can be explored through Monte Carlo and molecular mechanics simulations. In addition, to analyze the dynamics of this molecular rotor through variable temperature ^{2}H NMR spectroscopy, we prepared isotopically labeled samples with the two hydrogen atoms in the

central ring replaced by deuteria. As described below, ROT-2F has a slightly higher barrier to rotation than ROT-F and, despite a sterically symmetric rotational potential, an effective asymmetry suggests correlated steric and dipolar interactions.

II. EXPERIMENTAL DETAILS

A. Dielectric measurements

Two types of samples of ROT-2F are studied dielectrically: polycrystalline and single crystal. Electric fields are applied to the polycrystalline dipolar rotors using fabricated, gold, interdigitated capacitors on fused silica with a 15–20 nm titanium adhesion layer beneath an evaporated 200 nm gold film, as previously reported.[7] Each device has 25 fingers, 1 mm in length with 10 μm gaps between digits.

The single crystal samples are measured in a bulk capacitor consisting of two fused silica plates separated by three optics grade ruby ball lenses which provide a gap of 600 ± 2.5 μm. The facing sides of the plates contain pads made from evaporated Ti and Au with the same thickness as for the surface electrodes. The vapor-deposited pads are circular with a 5 mm radius producing a uniform field across the sample. A third fused silica plate, with one side coated with Ti/Au, is between the other two plates. The middle plate is grounded and has a hole through its center acting as a container for the sample as well as maintaining uniformity of the applied field. This geometry provides acceptable stability against temperature cycling and disassembly.

Three-dimensional polycrystalline samples are prepared from saturated solutions of ROT-2F rotor. 5 mg of the solid difluoro compound dissolved in 200 μL of dichloromethane yields a slightly supersaturated solution. Samples for dielectric use are grown by drop casting 0.6 μL of a saturated solution from a micropipet onto a surface capacitor. This volume yields a polycrystalline structure covering most of the active part of the capacitor. The single crystal grown for dielectric study is created by solvent diffusion from a dichloromethane/methanol mixture which leads to a sample mass of 0.29 mg.

Dielectric measurements are performed on the polycrystalline samples using a cryogenic probe station modified by adding a copper stage that can be temperature controlled independently of the cooling mechanism of the system. Surface capacitors are attached to the copper stage using Apiezon *L* grease and a copper clip. The system is then evacuated to less than 4×10^{-6} Torr and dielectric measurements are performed at 0.1, 1, and 10 kHz from 80–370 K with an Andeen-Hagerling 2700A ratio transformer capacitance bridge. Data sets include both increasing and decreasing temperature steps in 5 K intervals with a 5 min settling time for thermal equilibrium at each step. At each temperature and each frequency, five measurements are made with 30 s intervals. For single crystal dielectric measurements, the bulk capacitor and a reference capacitor of identical design are mounted on a stage in a vacuum can which is submerged in a cryostat. Measurements are taken at frequencies of 100, 400, and 1000 Hz with a Dekatran-based capacitance bridge.

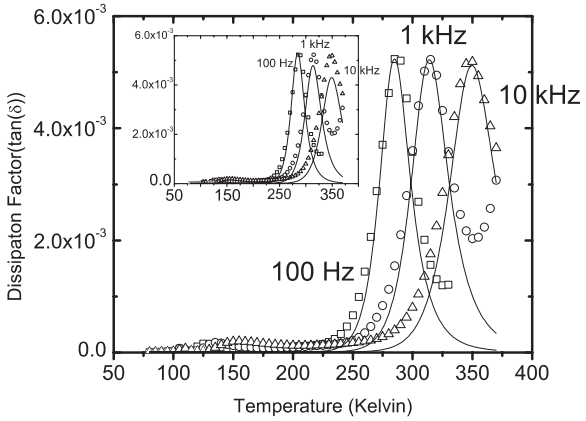

FIG. 4. Plot of tan(δ) versus temperature from ROT-2F with tan(δ) from a blank electrode subtracted (open symbols). The solid lines are single Debye peaks with barrier and attempt frequency values from the Arrhenius plot. The magnitude has been set by the 100 Hz peak and an asymmetry *S* of 0.9 kcal/mol chosen to fit the relative peak amplitudes. The inset shows the same plot with a fit where the asymmetry is zero.

B. Solid state ^{2}H NMR measurements

Solid state ^{2}H NMR measurements of ROT-2F are carried out on powders ground from large single crystals. A Bruker Advance instrument with a frequency of 46.073 MHz is used with a single channel solenoid probe containing a 5 mm insert. Measurements are made between 297 and 446 K, with temperature calibration using ^{195}Pb shift standard. The spectra are acquired with a quadrupole echo pulse sequence, where the 90° pulse width is 2.5 μs; echo and refocusing delays are 50 and 45 μs, respectively, and the recycle delay is 20 s between pulses. Exchange rates are determined by visually matching the experimental data with the simulated spectra. We calculate the model shape using the program reported by Nishikiori *et al.*[31] with a quadrupolar coupling constant (QCC) determined from spectra acquired in the slow exchange regime and a model that considers site exchange of the ^{2}H nuclei by 180° rotations. The only adjustable parameters are the site-exchange rate k_r and the population difference at each of the two nonequivalent sites, which is determined by the asymmetry parameter *S*, as defined in Fig. 3.

III. EXPERIMENTAL RESULTS

A. Dielectric measurements

A typical dielectric experiment consists of measuring the dissipation factor, or tan(δ), versus temperature on a blank surface capacitor, followed by deposition and measurement of the ROT-2F molecules. The dielectric loss data of the blank electrode are featureless and flat on the scale of the ROT-2F loss peaks. Spectra of background subtracted polycrystalline ROT-2F are shown in Fig. 4 as open symbols. There are two features in this data set to note. First, there are very large peaks occurring near room temperature. The location of each peak is increasing in temperature with increasing frequency and the 100 Hz data is peaked at 290 K, 1 kHz at

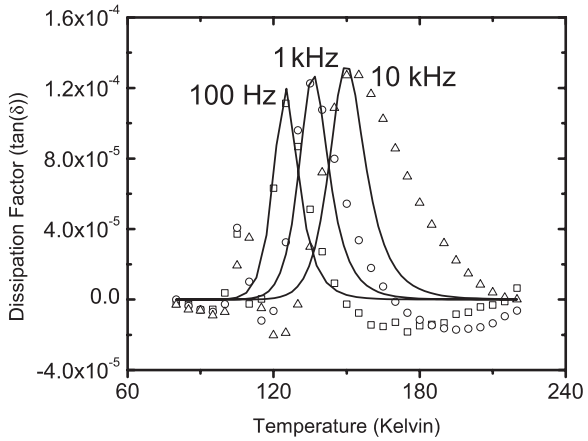

FIG. 5. Plot of $\tan(\delta)$ versus temperature for the lower temperature tail of ROT-2F with a linear background subtracted (open symbols). Also plotted is the single Debye fit to the data with E_B of 6.2 kcal/mol, ω_0 of 5.4×10^{14} s^{-1}, and asymmetry S of 5.5 kcal/mol.

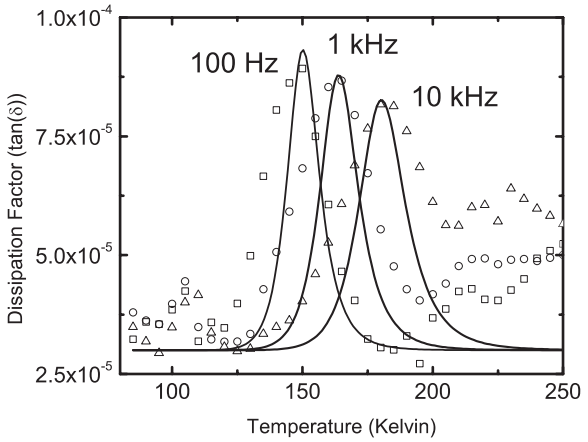

FIG. 6. Plot of dissipation factor versus temperature of the lower temperature tail of ROT-H with the dissipation from the blank electrode subtracted (open symbols). A single Debye fit with E_B of 8.2 kcal/mol, ω_0 of 5.4×10^{14} s^{-1}, and no well asymmetry is represented by the solid line at each frequency.

315 K and 10 kHz at 350 K. Also, there is structure seen in the low temperature tail of the ROT-2F data centered around 150 K. The structure is magnified in Fig. 5. All of these features are reproducible over many experimental depositions and in data collection with both increasing and decreasing temperature.

The low temperature structure in the ROT-2F dielectric data is highlighted in Fig. 5. The dielectric loss from the blank electrode has been subtracted at each temperature as well as a linear background slope from the ROT-2F data points. There are two sets of peaks shown in this figure. The larger structures are dispersing with frequency with the peaks located at 125, 135, and 145 K for 100 Hz, 10 kHz, and 10 kHz, respectively. These peaks differ from the ≈300 K features in Fig. 4 in that they increase in amplitude with increasing frequency while the 300 K peaks are constant in magnitude. There is also a small nondispersing structure at 105 K.

In order to distinguish behavior due to the central rotating dipole from bulk crystal effects, we also measure dielectric loss on a control molecule ROT-H, which contains no dipole moment in the central phenyl ring and is represented in Fig. 1. ROT-H does not show the large feature at ≈300 K, which we attribute to the dipolar central ring. At low temperatures, the dielectric data for ROT-H with the loss of the blank electrode subtracted is shown in Fig. 6. Here, the small nondispersing structure at 105 K seen in ROT-2F is evident as is a set of dispersing peaks around 160 K. The dispersing peaks occur at 150 K for measurements at 100 Hz, 165 K at 1 kHz and 180 K at 10 kHz. These structures have been seen at the same temperatures for several different depositions of the control molecule.

B. Solid state ^{2}H NMR measurements

The NMR data are also measured over a temperature range. The experimental results are shown as solid curves in Fig. 8. The line shape alters as the temperature is changed, which will be correlated to the averaging of molecular motion in Sec. IV C.

IV. ANALYSIS

A. Basic behavior of the system

Based on previous evidence and x-ray diffraction studies, the dielectric data is modeled by thermal hopping of the central dipolar group between the wells of a twofold potential curve. The rate of reorientation between the wells, defined as the reciprocal of the relaxation time τ is given as[32,33]

$$\frac{1}{\tau} = \omega_0 \exp\left(\frac{-E_B}{kT}\right). \tag{1}$$

Here, ω_0 is the attempt frequency (or libration frequency of the rotor in the well), k is Boltzmann's constant, and E_B is the barrier to rotation seen in Fig. 3. To be precise, the relaxation rate of the rotor will be the sum of the frequencies over all paths for rotation and the relaxation time will be the reciprocal of this sum, however the lowest barrier will dominate the relaxation in the systems presented here.[34]

B. Dielectric measurements

In dielectric spectroscopy, we measure dielectric loss, or $\tan(\delta)$, which is the ratio of the imaginary to real part of the dielectric constant. The real part alone yields similar information as the dielectric loss but is sensitive to variations in experimental setup and probe contact while the loss is robust to these factors. For an ideal capacitor filled with molecular rotors, the only source of loss will be from the motion of the rotor molecule leading to[35]

$$\tan(\delta) = \frac{C_R}{C_0}\frac{\omega\tau}{1+\omega^2\tau^2}. \tag{2}$$

The measurement frequency is ω and $1/\tau$ is the relaxation rate with the temperature dependence given by Eq. (1). The

electrode capacitance and that due to the nonrotating portion of the molecules is assumed lossless and given by C_0, which is typically near 1 pF. An explicit expression for the static capacitance of the rotating groups C_R can be given for an idealized situation: a parallel plate capacitor with area L^2 and gap L, completely filled with a homogenous dielectric material containing the polar rotors

$$C_R = \frac{\epsilon_R + 2}{3} \frac{Np_0^2}{3kTL^2} \cosh^{-2}\left(\frac{S}{2kT}\right). \quad (3)$$

Equations (2) and (3) predict a loss peak where the measurement frequency equals the hopping rate. The magnitude of the resultant peak depends on the number of rotors in the capacitor N, and the strength of the bare dipole moment p_0. In the dilute limit, the rotors are treated as if they are located in spherical cavities in the dielectric medium, which has a dielectric constant $\epsilon_R \approx 2$, giving rise to a local field correction factor $\frac{\epsilon_R+2}{3}$.[34] The $\cosh^{-2}$ factor accounts for suppression of the signal as the temperature decreases and the rotor population in the lower well increases.[36] Except for an overall numerical factor of order unity, which is not important for our purposes, we expect Eq. (3) to apply to the present data if we set L equal to the 10 μm gap. The value of N estimated for our samples from the geometry and crystal density is 1×10^{15}.

Due to the lack of large structures in the lineshape of the nonpolar ROT-H molecule as compared to the polar ROT-2F molecule, we attribute the room temperature dielectric loss peak in Fig. 4 to the central dipole. The peak in $\tan(\delta)$ occurs, according to Eq. (2), when the relaxation rate is equivalent to the measurement frequency, or $\omega\tau = 1$. This gives rise to an Arrhenius equation in which a plot of $\ln \omega$ versus $1/T_{\text{peak}}$, where T_{peak} is the temperature where the loss peak occurs, produces a line with slope E_B/k and y intercept of $\ln \omega_0$. The barrier, E_B, is found to be 14.1 ± 0.2 kcal/mol with an ω_0 of $4 \pm 1 \times 10^{13}$ s^{-1}. The barrier is slightly higher than the 13.6 kcal/mol value observed for the ROT-F rotor, perhaps due to greater steric hindrance by two F atoms instead of one.

With E_B and ω_0 given by an analysis of the peak locations, Eq. (2) can be used to fit the loss data with only two unknown parameters, the number of rotors in the field of the capacitor N and the asymmetry S. Fitting $\tan(\delta)$ data requires a unique combination of these parameters. Based on the symmetries of the ROT-2F structure discussed previously, one expects the asymmetry S to be zero if rotor-rotor interactions are not important. However, if S is set to 0 and N is fit to the 100 Hz peak, the dispersed peak heights do not match the data as is exemplified in the inset of Fig. 4. In fact, an asymmetry of 0.93 ± 0.01 kcal/mol is required to fit the data, as shown in Fig. 4. The number of dipoles found with this asymmetry is 7×10^{14} which is less than a factor of 2 below the estimate from deposition of 1×10^{15}. Below we explore several possible explanations for the observed asymmetry.

A further elucidation of the bulk effects versus the rotational group characteristics of the crystal requires analysis of the control data, ROT-H. The peaks seen in Fig. 6 have been fitted with a Debye response and the fit is shown by the solid curves. The same analysis as was performed on the large ROT-2F peak is repeated here giving a barrier to rotation $E_B = 8.2$ kcal/mol and $\omega_0 = 5.4 \times 10^{14}$ s^{-1}. There are two unknown quantities to determine the magnitude of the peaks, the dipole moment and number of active dipoles. These may be treated as a single variable. The same peaks in ROT-2F are fitted in Fig. 5. The location of these peaks is too low in temperature to affect the large ROT-2F peaks and their presence in the control ROT-H confirms that they are unrelated to the dynamics of the central ring.

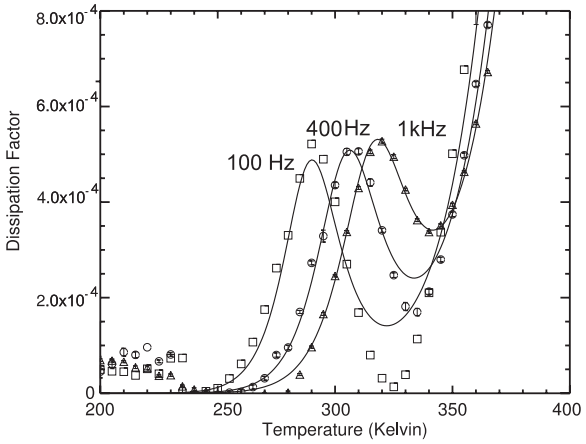

FIG. 7. Plot of dielectric data taken on a single crystal of ROT-2F. The data were taken at 100 Hz, 400 Hz, and 1 kHz. The fits are single Debye with $E_B = 15.1$ kcal/mol, $\omega_0 = 8 \times 10^{13}$ s^{-1}, and asymmetry $S = 0.9$ kcal/mol. The exponentially increasing loss above 330 K is fit to an ionic conductivity term.

There are no apparent polar groups seen in the control molecules to account for a reorienting electric dipole so the dipole moment of the object responding to the field must be very small. The origin of this dipolar motion is unknown. However, we would expect the dipole moment to reside in the triphenyl groups shown in gray in Fig. 1 since if it is associated with central phenyl ring, the barrier would have to be closer to 13 or 14 kcal/mol.

Another aspect of the dielectric loss data to be noted is the sharp rise in all data at the highest temperatures. These appear to be the effects of ionic conductivity. By fitting it to an exponential function, we find that it has no affect on the locations or magnitudes in the 14 kcal/mol peaks.

The measurements of the single crystal of ROT-2F does not yield data as reproducible as the measurements for the polycrystalline samples stemming from the movement of the crystal in the capacitor, so the smaller signals at lower temperature could not be resolved. However, in the next section we will analyze the source of the asymmetry in ROT-2F and show that both dipolar and random strain effects from disorder could theoretically cause an asymmetry. In order to differentiate these two effects, we analyze the large signal due the phenyl rotor in the single crystal sample. The dielectric data from the single crystal are shown in Fig. 7. The data show single Debye peaks with $E_B = 15.1 \pm 0.5$ kcal/mol and $\omega_0 = 8 \pm 4 \times 10^{13}$ s^{-1}. This is in agreement with the polycrystalline data. In addition, the asymmetry S is fitted with

0.9±0.5 kcal/mol, also in agreement with the polycrystalline data. The exponentially increasing loss above 330 K is fit to an ionic conductivity term of the form $\frac{A}{T}\frac{\exp(-E_\sigma/kT)}{\omega^s}$, where A is a prefactor, T is the temperature, E_σ is the barrier energy in a hopping model of ionic conductivity,[37] ω is the measurement frequency, and $0<s<1$.[38] The magnitude of the peaks is consistent with a sample containing 3×10^{17} rotor molecules, based on the molecular mass of the sample, whose rotational potential wells form an angle of 60° with respect to the applied electric field.

C. Solid state ^{2}H NMR measurements

The rotational dynamics in the solid state is also accessible by ^{2}H NMR spectroscopy. The ^{2}H NMR relies on the analysis of spectral changes caused by dynamic averaging of the orientation-dependent interaction between the ^{2}H nuclear electric quadrupolar moment and the electric field gradient (EFG) at the nuclear position. Each deuteron provides a doublet of peaks with a splitting frequency $\Delta\nu$ given by[39]

$$\Delta\nu = \frac{3}{4}\frac{e^2q_{zz}Q}{h}(3\cos^2\beta - 1) = \frac{3}{4}\mathrm{QCC}(3\cos^2\beta - 1). \quad (4)$$

Here, Q represents the electric quadrupole moment of the deuteron, e and h are the electric charge and Planck constant, respectively, and q_{zz} is the magnitude of the principal component of electric field gradient tensor, which lies along the C-^{2}H bond. The combination of these factors is commonly called the quadrupolar coupling constant (QCC). In a static polycrystalline sample, the isotropic distribution of the C-H bonds result in a typical powder pattern, or Pake pattern, with characteristic symmetric discontinuities due to the C-^{2}H bonds that are parallel or perpendicular to the external field. Variations in the powder pattern of a solid sample occur when the C-^{2}H bonds experience reorientations that reduce their orientation-dependent quadrupolar coupling by dynamic averaging in the intermediate exchange regime, which goes from $\approx10^4$ to 10^8 s^{-1}.

A sample of d_2-ROT-2F, prepared with two deuteria in central phenylene rotator, is measured as a function of temperature and analyzed as described previously. The experimental line shape is matched by simulated spectra obtained by using a QCC=168 kHz and a rate of exchange by 180° flips k_r that ranges from $k_r=1\times10^3$ Hz at 289 K to 1×10^7 Hz at 476 K (Fig. 8). Although the dielectric data suggested an asymmetry parameter S=0.9 kcal/mol, the resulting variations in population caused no significant variations in the simulated spectra. An Arrhenius plot with the rate and temperature data gives a linear fit with a barrier $E_B=14.8\pm1$ kcal/mol and an attempt frequency $\omega_0=8\pm6\times10^{13}$ s^{-1}, consistent with the Arrhenius parameters obtained from the dielectric data.

D. Analysis of attempt frequency

Comparisons can be made between the observed attempt frequency and a value estimated classically. If the rotor is librating in a two well, sinusoidal potential and the thermal

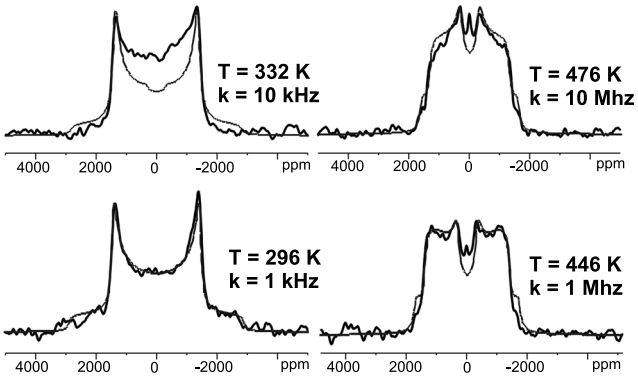

FIG. 8. ^{2}H NMR spectra. Experimental and simulated spectra for 180° flipping motion.

energy (kT) is much less than the barrier height (E_B) as is the case here, the libration frequency is[33]

$$\omega_0 = \sqrt{\frac{2E_B}{I}}. \quad (5)$$

Here, I is the rotational inertia of the phenylene group around its axis of rotation. Using a barrier of 14.1 kcal/mol and a rotational inertia calculated from point particles at the atoms' nuclear coordinates, the libration frequency is estimated to be 7×10^{12} s^{-1}, which is much less than the value obtained from the Arrhenius calculation of $4\pm1\times10^{13}$ s^{-1}.

The discrepancy between the experimental and the calculated attempt frequencies can be understood if there is a small linear temperature dependence of the rotational barrier E_B. If the rotational barrier is a well behaved function, it can be expanded as

$$E_B(T-T_0) = E_0 + \frac{E_1}{T_1}(T-T_0) + \cdots. \quad (6)$$

Here, T_0 is the temperature of interest where a peak occurs and E_0 is the barrier at T_0. If only the first two terms in equation (6) are considered, Eq. (1) becomes

$$\frac{1}{\tau} = \omega_0 \exp\left(\frac{-E_1}{kT_1}\right)\exp\left(-\frac{E_0 - \frac{E_1}{T_1}T_0}{kT}\right). \quad (7)$$

If we define an effective libration frequency ω_{eff} as

$$\omega_{\mathrm{eff}} = \omega_0 \exp\left(\frac{-E_1}{kT_1}\right), \quad (8)$$

and an effective barrier E_{eff} as

$$E_{\mathrm{eff}} = E_0 - \frac{E_1}{T_1}T_0, \quad (9)$$

then we may write Eq. (1) as[40]

$$\frac{1}{\tau} = \omega_{\mathrm{eff}} \exp\left(\frac{-E_{\mathrm{eff}}}{kT}\right). \quad (10)$$

The parameters ω_{eff} and E_{eff} are now the experimentally observable quantities of the system with ω_{eff} independent of

temperature. Based on the experimentally measured value of ω_{eff}, the slope of the barrier with temperature E_1/T_1, which is referred to as an entropic term,[33] is −0.003 kcal/mol/K. The effective barrier does not change with temperature. Thus, an apparently high attempt frequency is the only observable result from a small linear temperature dependence of the barrier height.

E. Calculations: Source of potential well asymmetry

The detection of a non-zero asymmetry S for the rotary potential ROT-2F rotation is unexpected based on the symmetry group of the rotor crystal, as discussed in Sec. I. We have two hypotheses for this result. The first is purely electrostatic interactions between the rotating dipolar groups within the crystal tending toward an ordered, polarized ground state. We explore this possibility using mean-field and Monte Carlo simulations. The second is indirect steric rotor-rotor interactions which we examine using molecular mechanics calculations. A third possibility could be a random field due to quenched disorder.[21] We have treated this scenario by parametrizing the random field and predicting the resulting dielectric spectra. However, if disorder were the culprit for the asymmetry observed, the single crystal dielectric data would be expected to show a decrease in this value. It thus seems unlikely that the observed effective asymmetry is due to quenched disorder. Therefore, the electrostatic and indirect steric possibilities will be addressed.

Each dipolar rotor is surrounded by identical dipole moments in an ordered three-dimensional arrangement. We will treat this as a system of point dipoles. The dimensions of the system are taken from the low temperature x-ray structure. The lattice is triclinic with lattice vectors a=9.18 Å, b =10.54 Å, c=10.55 Å and angles α=62.74°, β=70.90°, γ =85.37°. The lattice vectors are converted to Cartesian coordinates using the a vector as the x axis and the b vector lying in the x,y plane. In Cartesian coordinates the central rotating ring is treated as a point dipole with magnitude three Debye and occupying the allowable unit vector directions of (0.0312, 0.630, −0.776) and (−0.0312, −0.630, 0.776).

F. Mean-field approach

We first try to model this system with a mean field approximation. The ground state is calculated by finding the energy of a single dipole in the field created by the surrounding crystal lattice of electric dipoles. Using an Ewald-Kornfeld representation[41] of the dipolar interactions with one electric dipole per unit cell, the energy of a single dipole, labeled $\mathbf{p}_i$, in the field of the surrounding lattice of dipoles $\mathbf{E}_i$ is

$$\mathbf{p}_i \cdot \mathbf{E}_i = \sum_{\mathbf{R}\neq 0} [(\mathbf{p}_i \cdot \mathbf{p}_R)B(R) - (\mathbf{p}_i \cdot \mathbf{R})(\mathbf{p}_R \cdot \mathbf{R})C(R)] + \frac{4\pi}{V_c}\sum_{\mathbf{G}\neq 0}\frac{1}{G^2}\exp\left(-\frac{G^2}{4\eta^2}\right)(\mathbf{p}_i \cdot \mathbf{G})(\mathbf{p}_R \cdot \mathbf{G}) - \frac{4\eta^3 p_i^2}{3\sqrt{\pi}}. \quad (11)$$

$\mathbf{p}_R$ represents the dipole located at the point $\mathbf{R}$. V_c is the volume of the unit cell and $\mathbf{G}$ is the reciprocal lattice vector. η is an adjustable parameter chosen so that the summations over the real and reciprocal lattice converge quickly. B and C are given by

$$B(r) = \frac{\text{erfc}(\eta r)}{r^3} + \frac{2\eta}{\sqrt{\pi}r^2}\exp(-\eta^2 r^2), \quad (12)$$

$$C(r) = \frac{3\,\text{erfc}(\eta r)}{r^5} + \left(\frac{4\eta^3}{\sqrt{\pi}r^2} + \frac{6\eta}{\sqrt{\pi}r^4}\right)\exp(-\eta^2 r^2), \quad (13)$$

where erfc(r) is the complementary error function.[41]

The experimental observable calculated from Eq. (11) is the asymmetry a dipole would feel upon flipping between its wells, which is $2|\mathbf{p}_i \cdot \mathbf{E}_i|$. We explore various periodic configurations for the direction of $\mathbf{p}_j$ with the periodic element containing two unit cells. This does not preclude the existence of more complex states with periodicity spanning over a greater number of cells, but represents a reasonable hypothesis. It appears that the ground state configuration for the lattice is with parallel aligned dipoles along the b and c vectors, and antiparallel along the a vector. Thus it is an antiferroelectric ground state with parallel planes that switch orientation along the a vector direction as is shown in Fig. 9. This ensemble yields a ground state asymmetry of 1.4 kcal/mol.

The ground state provides the maximum field felt by each rotor leading to an asymmetry S_{gs}. As the temperature increases the polarization of the crystal will decrease as rotors with more thermal energy oscillate into unfavorable energy configurations, decreasing the asymmetry. Each rotor will experience different fields, but we may calculate the mean asymmetry for a given rotor as function of temperature to be[42]

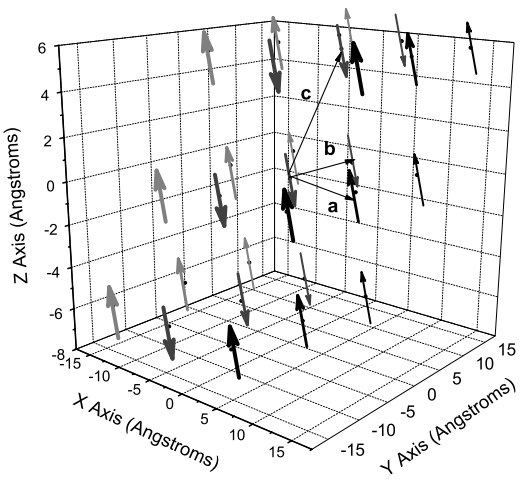

FIG. 9. Ground-state configuration of nearest-neighbor dipoles. Only alignment and not relative magnitudes are shown. For each dipole, line thickness decreases with position along the b axis, with dipoles at $-b$ the thickest. Similarly, dipole shade increases with position along the a axis, with dipoles at $+a$ the darkest. Within the c,b planes, a ferroelectric configuration is observed, while adjacent planes in the a direction switch orientation.

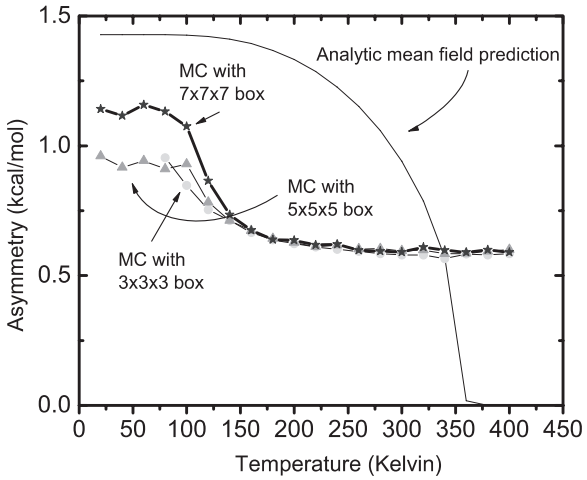

FIG. 10. Predicted temperature dependencies of asymmetry in rotor potential well. The black line is the prediction by mean field theory with the ground-state energy calculated by Eq. (11). The lightest gray circles and line are the results of a Monte Carlo (MC) simulation using the neighbors one lattice vector away from the center dipole, or a simulation box of $3\times3\times3$ dipoles. The darker gray triangles come from an MC simulation with a $5\times5\times5$ lattice of dipoles. Finally, the stars and line result from an MC simulation with all dipoles within three lattice vectors of the center dipole, or a $7\times7\times7$ simulation box.

$$S = S_{\text{g.s.}} \tanh\left(\frac{S}{2T}\right), \tag{14}$$

which is plotted in Fig. 10 using 1.4 kcal/mol as S_{gs}. Above the critical temperature (T_C), which is equal to the ground state energy, the asymmetry is averaged out to zero due to the rapid hopping of the dipoles into numerous configurations. However, below T_C the asymmetry increases with decreasing temperature until the ground state is reached at zero temperature.

Mean field theory provides a temperature dependent asymmetry which may be used to simulate dielectric loss data. We have used the analytically calculated asymmetry at 285 K to fit the magnitude of the 100 Hz peak of ROT-2F. Then, using the number of contributing rotors found, and the relevant asymmetry at the corresponding temperature, we have predicted the peak heights at 1 and 10 kHz. Qualitatively, one could imagine an asymmetry which decreases with increasing temperature may appear, experimentally, as a larger, temperature independent asymmetry. The lower temperature peaks would be progressively more suppressed. However, the theoretical temperature dependence predicted by a purely mean field method has too steep of a gradient to match the experimentally observed asymmetry. Possible ground states, and thus T_C values, were examined between 200 and 400 K none of which could produce the necessary constant magnitude behavior seen experimentally in Fig. 4.

G. Monte Carlo simulations

We may also find the asymmetry value using a Monte Carlo computer simulation at varying temperatures. This becomes a necessary step when the dielectric loss peaks occur near T_C. In the mean field case, if the central dipole of an array is surrounded by an ensemble of its neighbors yielding an interaction energy $(p\cdot E)$, and another dipole is surrounded by the inversely oriented field providing the inverse energy, the mean field method will sum those ensembles to zero. Experimentally, however, both of those ensembles lead to the same asymmetry, with only the orientation of the lowest well differing in the two cases. At low temperatures, both calculations should give the same results. Close to T_C, when the mean field tends to zero, the Monte Carlo calculation result will tend to a finite value.

This Monte Carlo simulation employs a Metropolis algorithm with 10 000 Monte Carlo steps at each temperature. First, only neighboring dipoles within a simulation box of one lattice vector, or a $3\times3\times3$ box of dipoles, were accounted for using their Coulombic energy. The calculation yields a distribution of asymmetries for an ensemble of 10 000 rotors in this case which is used to calculate the dielectric loss peak heights and then determine an effective single Debye asymmetry which is reported here. The results of the nearest neighbor Monte Carlo calculation are shown in Fig. 10 as the light gray data. There are three notable features. The first is the discrepancy in the ground state energy point at 20 K between the nearest neighbor calculation which does not account for long range interactions and the Ewald calculation. The second is the drop in asymmetry occurring much lower in temperature than in the mean field case. At these lower temperatures, the calculations should yield the same results. This behavior in the Monte Carlo is explained by the finite simulation box chosen. The dipoles on the edge of the box have less drive to polarize since they are surrounded by vacuum on the outside, thus they depolarize the ensemble at a much lower temperature than for an infinite lattice. Finally, as was expected, rather than averaging to zero above T_C, the Monte Carlo predicts a finite asymmetry of 0.6 kcal/mol above 200 K.

The same simulation is performed with boxes encompassing two and three lattice vector distances. The results are shown in Fig. 10. The more lattice shells used in the calculation, the larger the ground state asymmetry becomes, tending toward the analytic result. Also, the downward curve of the asymmetry occurs at higher temperatures with more simulation dipoles. At experimentally relevant temperatures close to 300 K, the predicted asymmetry remains temperature independent, as is observed in the experimental data, but with a smaller value of 0.6 kcal/mol. Therefore, even with expanding simulation cells, the resulting asymmetry between 285 and 350 K is still too small to account for the experimentally observed 0.9 kcal/mol.

Another effect which may raise the observed asymmetry would be enhancement of the dipolar effect. This could be attributed to rotor-lattice-rotor interactions. The dipolar groups may tend to align in the electrostatically favorable orientation due to a minimization of the steric interactions. In order to obtain an estimate of the dipolar strength necessary to produce an asymmetry of 0.9 kcal/mol, various dipole moments are used in the Monte Carlo calculation. The distributions of asymmetries felt by a large ensemble of molecules resulting from the simulation with a three lattice vec-

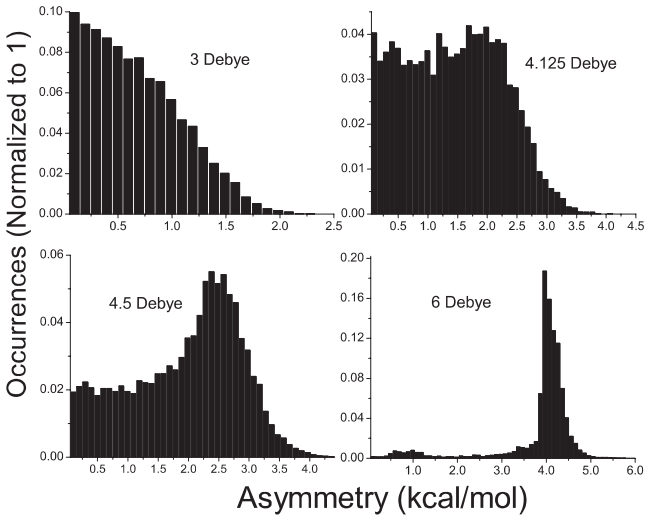

FIG. 11. Distributions of asymmetries for varying dipole interactions strengths. The distributions represent the ratio of dipolar rotors subject to the given asymmetry for the strength of dipole moment shown in the plots. The data is a results of 10 000 Monte Carlo steps at 300 K.

tor simulation box, or 343 dipoles, at dipole strengths of 3, 4.125, 4.5, and 6 D are shown in Fig. 11. These distributions were then used to create simulated dielectric data which was fitted with a single Debye peak to yield an effective asymmetry. With only a slight increase in dipole strength, the distribution locks into a ground state configuration, illustrated by the 6 D distribution. The correct effective asymmetry of 0.9 kcal/mol results for a dipole strength of 4.125 D.

Two possible corrections to the Monte Carlo simulation are the inclusion of long range dipolar interactions and the effects of higher multipole moments. The long range dipolar interactions may be accounted by using the Ewald-Kornfeld method again. The Monte Carlo Metropolis method is performed on the nearest neighbors of a center dipole, or a $3\times3\times3$ lattice. The total energy is calculated using a more general form of the Ewald formulation which is[41]

$$E_{\text{tot}} = \frac{1}{2}\sum_{i'=1}^{N}\sum_{j'=1}^{N}\sum_{\mathbf{R}}[(\mathbf{p}_i\cdot\mathbf{p}_j)B(r_{iRj}) - (\mathbf{p}_i\cdot\mathbf{r}_{iRj}) \times(\mathbf{p}_j\cdot\mathbf{r}_{iRj})C(r_{iRj})] + \frac{1}{2}\frac{4\pi}{V_c}\sum_{\mathbf{G}\neq0}\frac{1}{G^2}\exp\left(-\frac{G^2}{4\eta^2}\right) \times|\mathbf{M}(G)|^2 - \frac{1}{2}\frac{4\eta^3}{3\sqrt{\pi}}\sum_{i=1}^{N}p_i^2. \quad (15)$$

N is the number of rotors in a simulation box, which for the nearest-neighbor case is 27. A schematic of the simulation in two dimensions is shown in Fig. 12 where the simulation box is outlined and N is 9. The prime indicates all i, j except $i=j$ when $\mathbf{R}=0$, where $\mathbf{R}$ is the vector connecting simulation boxes to the center box. $\mathbf{p}_i$ and $\mathbf{p}_j$ represent all the dipoles in the simulation box and $\mathbf{r}_{ij}$, in Fig. 12, is the distance between them. $\mathbf{r}_{iRj}$ in Eq. (15) is the sum of $\mathbf{R}$ and $\mathbf{r}_{ij}$ which is the total real distance between dipoles in the simulation. Again,

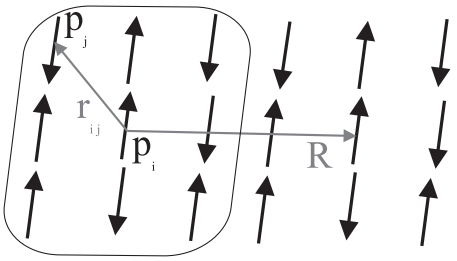

FIG. 12. A 2D schematic slice of the lattice used for the Ewald-Kornfeld calculation. The skewed rectangle represents the simulation box in which the Metropolis method is used to find the correct energy ensemble of dipole directions. $\mathbf{p}_i$ and $\mathbf{p}_j$ are arbitrarily chosen dipoles with $\mathbf{r}_{ij}$ giving the distance between them. $\mathbf{R}$ is the distance between the simulation box at the origin and any arbitrary box, with the neighboring box being shown here.

η is chosen so that the sums over $\mathbf{R}$ and $\mathbf{G}$ both converge rapidly. Finally, $\mathbf{M}(G)$ is given by[41]

$$\mathbf{M}(G) = \sum_{i}^{N}\mathbf{p}_i\cdot\mathbf{G}\exp(i\mathbf{G}\cdot\mathbf{r}_{ij}). \quad (16)$$

Once a configuration is chosen by the Metropolis method using the total energy, the field on the center dipole is then calculated yielding the asymmetry as was done earlier. This calculation is computationally expensive, but results of a nearest neighbor simulation box at the temperatures where the ROT-2F peaks occur yields no change in the previous results. These results indicate that at experimentally relevant temperatures, the dipolar asymmetry is a nearest neighbor effect. We note that our calculations do not include dielectric screening by the bulk crystal and thus represent an upper bound on the dipolar effect. However, since the effect we are interested in is dominated by nearest neighbors, the dielectric screening is likely to be a small effect. If a larger simulation box were employed and the calculation performed at a range of temperatures, we expect the Monte Carlo method to reproduce the analytic mean field plot in Fig. 10 more closely at low temperatures. In addition to the long range interactions, higher multipole moments were calculated for ROT-2F using Gaussian 98 and translated to the center of the rotating phenyl ring. The inclusion of higher moments also had no effect on the electrostatic result.

H. Molecular mechanics simulations: Correlated sterics

The Monte Carlo simulation predicts a well asymmetry of 0.6 kcal/mol (300 K), less than the experimentally observed asymmetry of 0.9 kcal/mol. This simulation only includes electrostatic interactions without screening; it is based on the assumption that the asymmetry S must come from dipole-dipole interactions, because in the absence of interactions, the structural symmetries demand that $S=0$. The x-ray structure shows that nearest neighbor rotors are too distant from one another to have direct steric interactions. However, there might be indirect steric interactions mediated by local distortions of the lattice. The 0.3 kcal/mol discrepancy may arise from such an interaction.

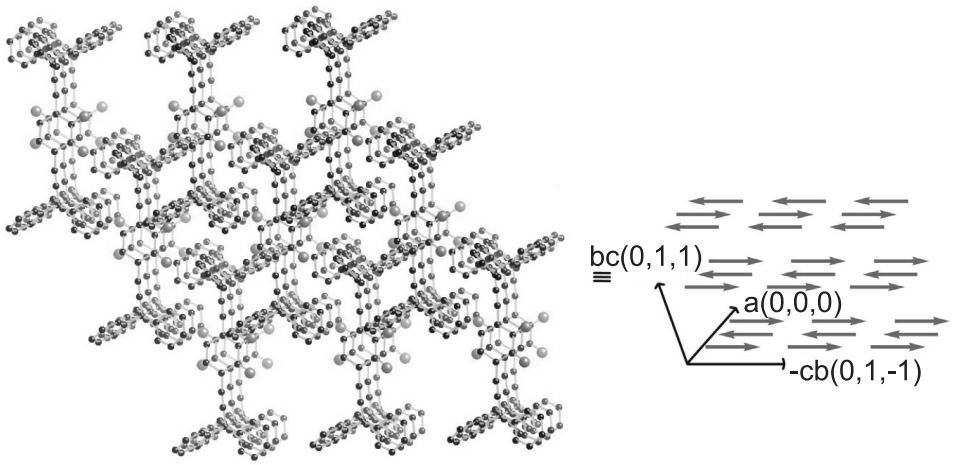

FIG. 13. Model $3\times3\times3$ grid of difluoro molecular rotors (hydrogen atoms not shown) (left). Schematic representation of the model depicting the relative orientation of dipoles. Relevant axes are shown (right).

As an attempt to test the feasibility of this mechanism, the energies of the upper and lower wells for the ROT-2F rotor are modeled with molecular mechanics using the MM3* force field.[43] A $3\times3\times3$ grid of molecular rotors is employed as the model system. It is built directly from crystallographic data and represents the same configuration as used in the Monte Carlo simulations, except now the rotors are included explicitly and potential energies are the sum of electrostatic (dipole-dipole effects) and steric (core repulsion and van der Waals interactions) terms in the mechanics force field (Fig. 13).

Rigidity due to the infinite crystal lattice is imposed with artificial geometric constraints. The relative positions of all 26 surrounding rotor molecules are translationally constrained by fixing the position of their methano triphenyl carbons. In order to maintain the torsional orientation of these triphenyl groups, the positions of the carbon atoms adjacent to each methano center are fixed. These fixed parameters were applied to all trityl groups except for those of the central rotor and the six trityl groups that interpenetrate and make contact with its central phenylene moiety. In this way, the core of the model is left unconstrained, but held loosely in place by the outer shell of fixed molecules. The constraints are applied using the standard, default force constant of 100 kJ/mol Å.[44] The energy is minimized with the central dipole in the lower and upper well orientations using the conjugate gradient PRCG method with an RMS convergence threshold of 0.05 Å. The electrostatic cut off is set to a 20 Å radius.

Monte Carlo calculations that would sample all the possible dipole configurations are not computationally feasible for this method. Indeed, there are about thirty four million possible configurations after symmetry is taken into account. Each calculation requires roughly two minutes of computer time. Since a complete automated and systematic approach is not feasible, a few select configurations shown in Fig. 14 are chosen.

These configurations are built on the assumption that adjacent dipoles along the crystallographic $-cb$ diagonal (0,1-1) formed looking down the a axis will have a strong preference to be ferroelectric (dipoles on the horizontal in Figs. 13 and 14). These dipoles are closest according to the structural parameters. Adjacent dipoles along the bc diagonal (vertical) and the a axis (perpendicular to the plane of the paper) interact less strongly. Only combinations of antiferroelectric and ferroelectric sheets are considered which match the results of long range and Monte Carlo calculations. There are twenty such combinations, after model symmetry is factored in. The asymmetries S for each configuration are deconstructed into steric S_s and electrostatic S_e components. In general, $S=S_s+S_e$. As expected, there is large variability in S_e with a mean absolute deviation (MAD) of 0.12. Surprisingly, this variability is also manifest in S_s (MAD=0.24). The electrostatic term is always the same sign as S (all asymmetries are given as upper or lower well). The steric term can be either positive or negative. Boltzmann weighting of these numbers at 300 K gives a value of $S=1.07$ kcal/mol, near the experimental value. The Boltzmann weighted S_e is 0.82 kcal/mol, slightly larger than that determined from Monte Carlo simulations. Finally, the weighted value for S_s is positive and has a magnitude of 0.15 kcal/mol. This asymmetry is assigned to dipole-lattice-dipole interactions. It is the right magnitude to account for the discrepancy between the Monte Carlo simulations and experiment. Although, a limited set of configurations is tested, these computations do establish the possibility of steric asymmetry, despite lattice symmetry, thus increasing the dipole-dipole interaction.

V. CONCLUSION

We have studied the rotational potential energy curve for a three-dimensional crystal of dipolar molecular rotors and have found evidence of direct dipole-dipole interactions. Molecular rotors comprised of the ROT-2F molecules rotate in a two well potential evidenced by low temperature x-ray data with the minima separated by 180°. Dielectric spectroscopy of both polycrystals and single crystals of ROT-2F along with solid state ^{2}H NMR studies provided complementary frequency regimes to characterize the rotation dynamics. ROT-2F was found to be subject to a 14–15 kcal/mol barrier

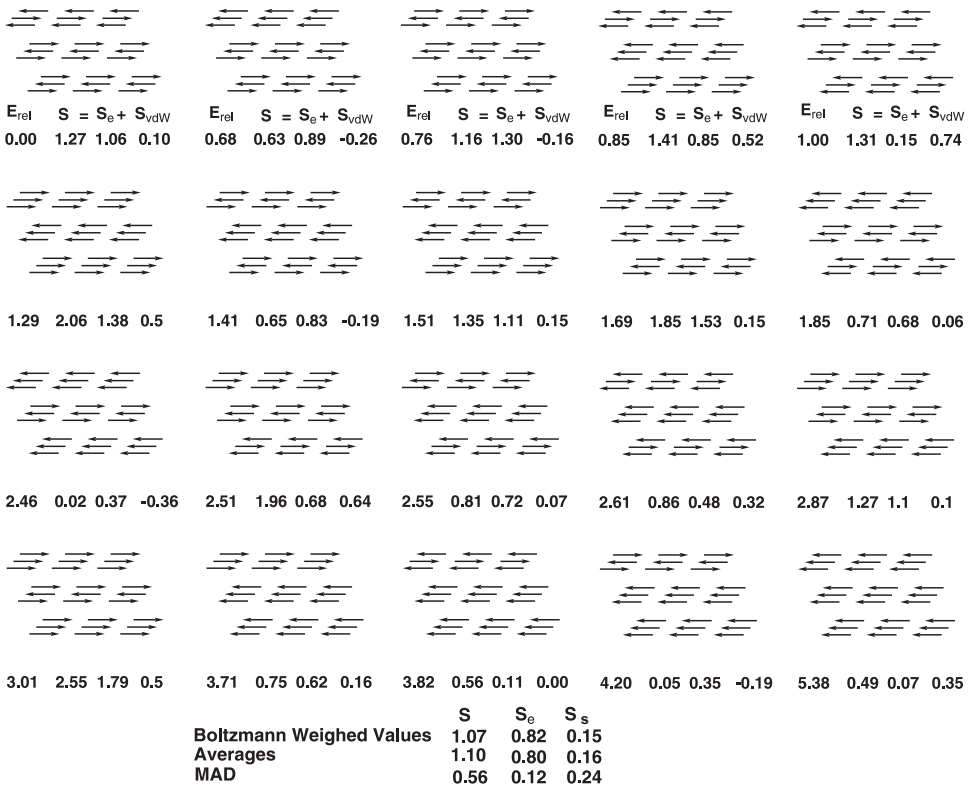

FIG. 14. Twenty dipole configurations used to calculate Boltzmann weighted asymmetries of the total difference in the two potential minima S, the difference due to only electrostatic interaction between dipole moments of the rotors S_e, and the difference due to steric interactions S_s. The configurations are presented in order of increasing relative energy (E_{rel}). Boltzmann weighted values are given at 300 K along with the average and mean absolute deviation.

to reorientation and an attempt frequency of $4-8\times10^{13}$ s^{-1}. In addition, an unexpected asymmetry in the energies of the rotational minima was detected which we explored with various modeling techniques.

The molecular and crystal symmetries of collections of ROT-2F yield a symmetric rotational potential energy curve when the effects of the surrounding lattice are spatially averaged. Yet, the large magnitude signal and sensitivity of the dielectric measurements showed an asymmetry of 0.9 kcal/mol. We explored three different possibilities for the source of this asymmetry: dipole-dipole electrostatic interactions, quenched disorder in the crystal, and rotor-lattice-rotor steric interactions.

Both mean-field and Monte Carlo calculations were used to model the effect of the molecular dipoles on one another in both the long and short range. We showed that short range, dipolar electrostatic interactions account for a significant portion of the observed effective asymmetry $\approx$0.6 kcal/mol. An alternative explanation, that the asymmetry arises from strain in the crystal caused by quenched disorder was shown to be plausible numerically, but was experimentally discarded since both single crystal and polycrystalline dielectric data yielded the same magnitude of asymmetry. Finally, molecular mechanics simulations provided motivation for the source of the remaining asymmetry above that expected for the electrostatics of rotating point dipoles. Steric interactions between neighboring rotating groups mediated through the bulk crystal showed a preferred alignment coincident with that shown by dipolar interactions and enhance the dipole-dipole effect.

Molecular rotors should provide a useful tool in creating nanometer scale machines and phenomena. We have shown here the ability to characterize the dynamics of organized, three-dimensional arrays of these molecules. In addition, the asymmetry of the rotational potential makes a good metric for tuning the rotor-rotor interactions in the molecular array, which show promise to provide novel behavior.

ACKNOWLEDGMENTS

Work at the University of Colorado was supported by the U.S. Army Research Office (Grant No. DAAD19-01-1-0521).

*Currently at Department of Physics, North Carolina State University
†Currently at Departamento de Quimica, Centro de Investigacion y de Estudios Avanzados del IPN Mexico D. F., 07000

[1] J. M. Tour, *Molecular Electronics* (World Scientific, New Jersey, 2003).
[2] V. Balzani and M. Venturi, *Molecular Devices and Machines: A Tour Into the Nano World* (Wiley-VCH, Winheim, 2003).
[3] J. Vacek and J. Michl, Proc. Natl. Acad. Sci. U.S.A. **98**, 5481 (2001).
[4] J. Gimzewski, C. Joachim, R. R. Schlittler, V. Langlais, H. Tang, and I. Johannsen, Science **281**, 531 (1998).
[5] G. S. Kottas, L. I. Clarke, D. Horinek, and J. Michl, Chem. Rev. (Washington, D.C.) **105**, 1281 (2005).
[6] R. D. Horansky, L. I. Clarke, J. C. Price, Tinh-Alfredo V. Khuong, P. D. Jarowski, and M. A. Garcia-Garibay, Phys. Rev. B **72**, 014302 (2005).
[7] L. I. Clarke, D. Horinek, G. S. Kottas, N. Varaska, T. F. Magnera, T. P. Hinderer, R. D. Horansky, J. Michl, and J. C. Price, Nanotechnology **13**, 533 (2002).
[8] Z. Dominguez, H. Dang, M. J. Strouse, and M. A. Garcia-Garibay, J. Am. Chem. Soc. **124**, 7719 (2002).
[9] Z. Dominguez, T.-A. V. Khuong, H. Dang, C. N. Sanrame, J. E. Nunez, and M. A. Garcia-Garibay, J. Am. Chem. Soc. **125**, 8827 (2003).
[10] V. Rozenbaum, V. Ogenko, and A. Chuiko, Sov. Phys. Usp. **34**, 883 (1991).
[11] K. Kim and N. S. Sullivan, Phys. Rev. B **55**, R664 (1997).
[12] J. de Jonge, M. Ratner, and R. S. S. W. de Leeuw, J. Phys. Chem. B **108**, 2666 (2004).
[13] G. Desiraju, *Crystal Design: Structure and Function, Perspectives in Supramolecular Chemistry* (Wiley, Chichester, 2003), Vol. 7.
[14] A. Gavezzotti, *Theoretical Aspects and Computer Modeling of the Molecular Solid State, The Molecular Solid State* (Wiley, Chichester, 1997), Vol. 1.
[15] S. I. Stupp, V. LeBonheur, K. Walker, L. S. Li, K. Huggins, M. Keser, and A. Amstutz, Science **276**, 384 (1997).
[16] V. A. Russell, C. C. Evans, W. Li, and M. D. Ward, Science **276**, 575 (1997).
[17] G. R. Desiraju, Angew. Chem., Int. Ed. **34**, 2311 (1995).
[18] J. Dunitz, E. Maverick, and K. N. Trueblood, Angew. Chem., Int. Ed. **27**, 880 (1988).
[19] J. Atwood, J. Davies, and ed. D. D. MacNicol, *Inclusion Compounds* (Academic Press, London, 1984).
[20] V. Balzani, *Supramolecular Chemistry*, edited by L. De Cola (Academic Press, London, 1984).
[21] J. Ortiz-Lopez, M. S. Li, and F. Luty, Phys. Status Solidi B **199**, 245 (1997).
[22] M. Garcia-Garibay, Proc. Natl. Acad. Sci. U.S.A. **102**, 10771 (2005).
[23] G. Gray and P. Winsor, *Liquid Crystals and Plastic Crystals* (Ellis Horwood, Chichester, 1974).
[24] C. Brot and I. Darmon, J. Chem. Phys. **53**, 2271 (1970).
[25] H. Kolodziej, P. Freundlich, S. Sorriso, and C. Sorriso, Chem. Phys. Lett. **305**, 375 (1999).
[26] C. Yannoni, R. Johnson, G. Meijer, D. Bethune, and J. Salem, J. Phys. Chem. **126**, 4540 (1991).
[27] J. Ortiz-Lopez and F. Luty, Phys. Status Solidi B **228**, 893 (2001).
[28] B. Koiller, M. A. Davidovich, L. Scavarda do Carmo, and F. Luty, Phys. Rev. B **29**, 3586 (1984).
[29] K. Okuyama, T. Hasegawa, M. Ito, and N. Mikami, J. Phys. Chem. **88**, 1711 (1984).
[30] V. A. Sipachev, L. S. Khaikin, O. E. G. V. S. Nikitin, and M. Traettberg, J. Mol. Struct. **523**, 1 (2000).
[31] S. Nishikiori, T. Soma, and T. Iwamoto, J. Inclusion Phenom. **27**, 233 (1997).
[32] N. G. McCrum, B. E. Read, and G. Williams, *Anelastic and Dielectric Effects in Polymeric Solids* (Dover Publications, New York, 1991).
[33] K. A. Dill and S. Bromberg, *Molecular Driving Forces* (Garland Science, New York, 2002).
[34] H. Frohlich, *Theory of Dielectrics* (Clarendon Press, Oxford, 1958).
[35] F. Kremers and A. Schonhals, *Broadband Dielectric Spectroscopy* (Springer-Verlag, Berlin, 2002).
[36] P. Debye, *Polar Molecules* (The Chemical Catalog Company, New York, 1929).
[37] D. L. Sidebottom, P. F. Green, and R. K. Brow, J. Non-Cryst. Solids **222**, 354 (1997).
[38] B. Lestriez, A. Maazouz, J. F. Gerard, H. Sautereau, G. Boiteux, G. Seytre, and D. E. Kranbuehl, Polymer **39**, 6733 (1998).
[39] N. Chandrakumar, *Spin-1 NMR* (Springer-Verlag, Berlin, 1996).
[40] N. Mott and R. Gurney, *Electronic Processes in Ionic Crystals* (Oxford, London, 1953).
[41] D. Frankel and B. Smit, *Understanding Molecular Simulation* (Academic Press, San Diego, 2002).
[42] C. Kittel, *Introduction to Solid State Physics* (Wiley, New York, 1996).
[43] N. L. Allinger, Y. H. Yuh, and J.-H. Lii, J. Am. Chem. Soc. **111**, 8551 (1989).
[44] F. Mohamadi, N. Richards, W. C. Guida, R. Liskamp, M. Lipton, C. Caufield, G. Chang, T. Hendrickson, and W. Still, J. Comput. Chem. **11**, 440 (1990).